Nonlinear Optics in Hydrogenated Amorphous Silicon

Kangmei Li, student member, and Amy C. Foster, member

Abstract—Nonlinear photonic circuits with the ability to generate and process signals all-optically have emerged in the past decade with superior performance to electronic chips. In particular, crystalline silicon has become a leading platform for integrated nonlinear optics. More recently, hydrogenated amorphous silicon emerged as a promising alternative to crystalline silicon due to its large nonlinearity. In this paper, we review recent research on nonlinear optical interactions in and applications of hydrogenated amorphous silicon nanophotonic devices. This new material platform enables the capability of multilayer CMOS-compatible photonic integrated circuits with low power requirements for high-speed optical signal processing.

Index Terms—Integrated optics, nonlinear optics, nonlinear optical devices, optical materials.

I. INTRODUCTION

ALL-optical signal processing is a key technology for future communication networks and promises to facilitate high speed and low power communication systems. By processing signals all-optically, the communication rate can be increased beyond 1 Tb/s [1][2]. During the past few decades, photonic-chip-based all-optical processing devices have enabled a wide range of capabilities, such as all-optical wavelength conversion [3]–[7], net on-chip parametric gain [8], signal regeneration [9][10], pulse characterization [11], logic functions [12][13], switching [14]–[16] and demultiplexing [17][18] at speeds far beyond the capabilities of electronic devices. To this end, a promising way to realize all-optical processing is through the use of ultrafast parametric nonlinear effects.

Producing nonlinear optical devices on an integrated platform can provide benefits in terms of footprint, cost, performance and power consumption [19]–[21]. Among all the platforms for integrated photonics, crystalline silicon (c-Si), typically in the form of silicon-on-insulator (SOI), has drawn considerable interest, mainly due to the combination of high refractive index, high third-order nonlinear (Kerr) coefficient n_2 , the ability to be mass-produced by the mature complementary metal-oxide-semiconductor (CMOS) technology, and the corresponding ability to combine photonics and electronics on the same chip. Integrated silicon photonic devices have demonstrated a vast array of functionality including wavelength conversion [22], signal regeneration [23],

Manuscript received February 14, 2018. This work is supported by the National Science Foundation.

optical logic [13][24], switching [14], transceiver systems [25][26], and optical links [27], indicating their versatility in information handling applications.

While c-Si exhibits many attractive optical properties, one main drawback for realizing nonlinear functionalities at the telecommunications band (around a wavelength of 1550 nm) is the low nonlinear figure of merit (FOM), defined as FOM = $n_2/(\beta_{TPA} \cdot \lambda)$, where β_{TPA} is the two-photon absorption (TPA) coefficient and λ is the wavelength. Not only is TPA directly responsible for optical loss through the absorption of two photons, but it also generates free carriers, resulting in undesired free-carrier absorption (FCA) and free-carrier dispersion (FCD). In order to alleviate the deleterious effect of TPA and achieve higher nonlinear FOM and hence higher efficiency of nonlinear interactions, materials with higher Kerr coefficient n_2 and lower TPA coefficient β_{TPA} are desired, as indicated by the established nonlinear FOM. Another disadvantage of c-Si is the high temperature growth process, thereby making it impractical to fabricate multilayer devices at the backend of existing CMOS electronics.

Hydrogenated amorphous silicon (a-Si:H) has been studied for many years for its application in solar cells, yet recently has emerged as a suitable material for nonlinear optical applications due to its high Kerr coefficient [3][4][28][29] and relatively low TPA coefficient, thereby yielding a high nonlinear FOM. Though these parameters can change depending on the growth conditions, its Kerr coefficient can be one order of magnitude larger than that of c-Si. In addition, a-Si:H films can be deposited at a low temperature (typically 200 - 400 °C) and patterned by the same technology as c-Si, making them compatible with back-end-of-the-line (BEOL) CMOS technology and therefore an attractive material for multilayer integration.

In this paper, we will first review many of the demonstrations of a-Si:H waveguiding devices for all-optical processing applications as well as their corresponding optical properties. Then, we will introduce new demonstrations in a-Si:H devices by our group. The paper is organized as follows: in section II the deposition and optical properties of a-Si:H devices are described; section III reviews seminal reports of a-Si:H nanophotonics devices for nonlinear applications; section IV shows our recent realization of high-speed logic gates using an a-Si:H waveguide; section V highlights our recent nonlinear

Kangmei Li and Amy C. Foster are with Johns Hopkins University, Baltimore, MD 21218 USA (e-mail: kli21@jhu.edu; amy.foster@jhu.edu).

four-wave mixing (FWM) results in an a-Si:H microring resonator; in section VI, the challenges and opportunities of a-Si:H for future nanophotonic applications are discussed; and finally the paper concludes in section VII.

II. A-SI:H PROPERTIES

Unlike the high-temperature epitaxial growth process of c-Si, a-Si:H can be readily deposited by plasma-enhanced chemical vapor deposition (PECVD). During the deposition process, the chamber is maintained at a low pressure of several hundred millitorr, silane (SiH₄) is diluted in inert gas (usually helium or argon) and serves as the source of silicon and hydrogen atoms, the substrate is kept at low temperature (typically 200-400 °C), and RF power is used to generate the plasma and catalyze the growth process. A simplified structure of a-Si:H is illustrated in Fig. 1. As is shown, the silicon atoms are not arranged in an ordered structure, meaning this material does not have a crystal lattice. This disorder results in an unsatisfied valance on some silicon atoms, typically called dangling bonds. Dangling bonds can cause absorption loss and defect states in the bandgap, and hence impair the performance of a-Si:H devices. Fortunately, the hydrogen atoms in SiH₄ help to passivate some dangling bonds by forming Si-H bonds, as depicted in Fig.1. Due to its similar chemical composition to c-Si, once deposited, devices can be created in a-Si:H films using the same processing steps as c-Si.

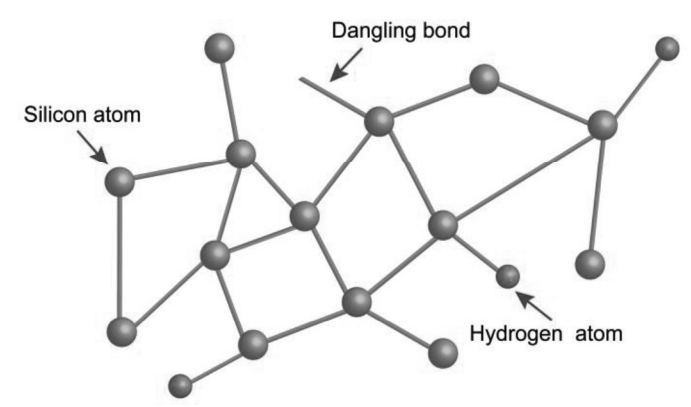


Fig. 1 Simplified structure of a-Si:H.

One important parameter to characterize the efficiency of third-order nonlinear effects in waveguides is the effective nonlinearity, γ , defined as $\gamma = \omega n_2/cA_{eff}$, where ω is the frequency of the photon, c is the speed of light, and A_{eff} is the waveguide effective area. From this relationship, it is clear that a higher n_2 and smaller A_{eff} are desired to increase the efficiency of the nonlinear optical process.

As a non-crystalline solid, the exact structure, elemental concentrations and optical properties of a-Si:H vary depending on the specific deposition conditions. However, previous reports generally show a high refractive index of 3.4-3.6 [4][15][28][30], comparable to that of c-Si. The high index contrast between a-Si:H and silicon dioxide makes it possible to strongly confine light in a small waveguide geometry (on the order of 100's of nm in both dimensions) and hence obtain small waveguide effective area A_{eff} and high light intensity in

the waveguide, which are critical for nonlinear optical interactions. Similar to c-Si waveguides, the linear loss of a-Si:H waveguides can be near $1-4\ dB/cm$ [3][4][15][28][31][32][33], originating from the material absorption as well as the device fabrication process.

The third-order nonlinearity of a-Si:H is generally reported to be much higher than that of c-Si. The Kerr coefficient n_2 of c-Si ranges from $0.28 \times 10^{-17} \, m^2 / W$ to $1.45 \times 10^{-17} \, m^2 / W$ as reported, and the β_{TPA} value is typically around 0.44 cm/GW to $0.9 \, cm/GW$ [34][35]. In comparison, n_2 of a-Si:H is often than $1 \times 10^{-17} \, m^2 / W$ be greater reported to [4][15][28][31][32][33][36][37] with values as high as $7.43 \times 10^{-17} \, m^2 / W$ [3][40], and the TPA coefficient β_{TPA} varying from negligible values to 7 cm/GW, as summarized in Table 1. This large variation of nonlinear properties results from difference in the structure and elemental concentrations of a-Si:H films, and is closely related to the band gap energy E_q of the material. According to Dinu's model [36][38], the values of n_2 and β_{TPA} depend on the ratio between the photon energy $E_p = \hbar \omega$ and the band gap energy E_g . Therefore, tuning the band gap of a-Si:H film using techniques described in [39] can have a great effect on the nonlinear properties. The theoretical results in [38] show that when $E_p/E_q < 0.7$, β_{TPA} drops at a much faster rate than n_2 with decreasing E_p/E_q . This implies that one can optimize the nonlinear performance of a-Si:H devices by changing the material deposition processing conditions and hence the band gap energy: for applications that require low power consumption, high Kerr coefficient can be achieved by narrowing the band gap (though the TPA coefficient might be high); while for applications requiring high nonlinear FOM, the performance can be improved by increasing the band gap of the material. As reported in [29][31][32], the nonlinear FOM of a-Si:H devices can be increased from 0.66 to 5, with n_2 decreasing from $4.2 \times 10^{-17} \, m^2 / W$ to $2.1 \times 10^{-17} \, m^2 / W$ and β_{TPA} dropping from $4.1 \, cm/GW$ to $0.25 \, cm/GW$.

TABLE 1 NONLINEAR CHARACTERISTICS REPORTED FOR A-SI:H WAVEGUIDES

Ref.	$n_2 [10^{-17} m^2/W]$	$\beta_{TPA} [cm/GW]$	$\gamma [W^{-1}m^{-1}]$	FOM
[3][40]	7.43	N/A	3000	N/A
[4]	5	7	2000	0.46
[15]	1.0	0.14	N/A	4.7
[18][41]	0.3	0.2	N/A	0.97
[28][33]	1.3	0.39	770	2.1
[29]	1.75	0.23	332	4.9
[30]	0.05	0.08	35	0.4
[31]	2.1	0.25	1200	5
[32]	4.2	4.1	2003	0.66
[36]	2.2	Negligible	N/A	N/A
[37]	2.8	N/A	790	3.06
[42]	N/A	Negligible	N/A	N/A

III. DEMONSTRATIONS

The outstanding nonlinear optical properties of a-Si:H have resulted in a significant amount of research over the last several years exploring the potential of utilizing a-Si:H devices for alloptical applications.

A. Self-Phase Modulation

When a high-intensity optical pulse propagates within a third-order parametric nonlinear optical medium, a nonlinear phase shift with the same temporal shape as the optical pulse intensity is experienced by the pulse. This effect is typically described in terms of an intensity dependent change in the refractive index $\Delta n = n_2 I$, where I is the optical intensity and is known as self-phase modulation (SPM). As a consequence of the nonlinear phase shift, SPM usually leads to spectral broadening. SPM is also an efficient way to characterize the Kerr coefficient n_2 ; at the same peak power higher n_2 leads to larger nonlinear phase shift and thus greater spectral broadening. Several SPM demonstrations [31][32] have been made using a-Si:H devices, here we show the results in [32] as an example. A nonlinear phase shift of 3.5π is obtained at 4.1 W coupled input peak power in a 7-mm long a-Si:H waveguide; the corresponding spectrum is shown in Fig. 2 where the normalized transmission above -10 dB spreads approximately 200 nm in the spectrum. In comparison, SPM experiments in a c-Si waveguide show that a peak power of 110 W is required to achieve a nonlinear phase shift of 2π , and the normalized transmission above -10 dB spreads only about 10 nm [43]. The larger n_2 value in the a-Si:H device provides a larger nonlinear phase shift with significantly less peak powers than a comparable c-Si device, thereby reducing the power requirements for the interaction.

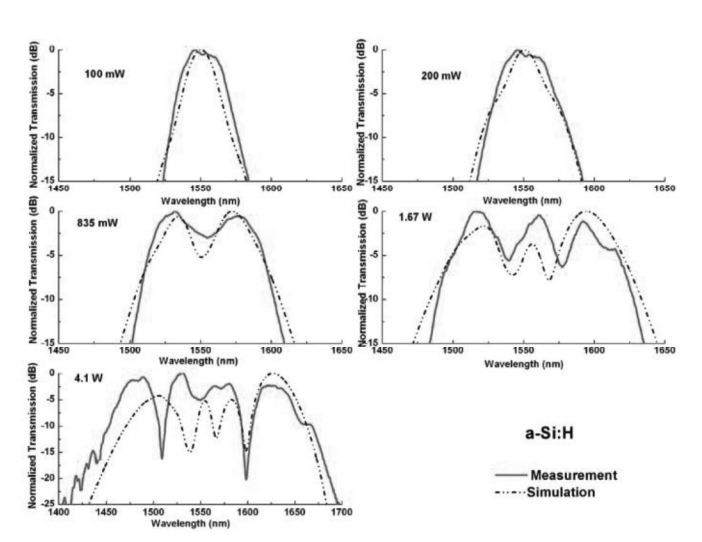
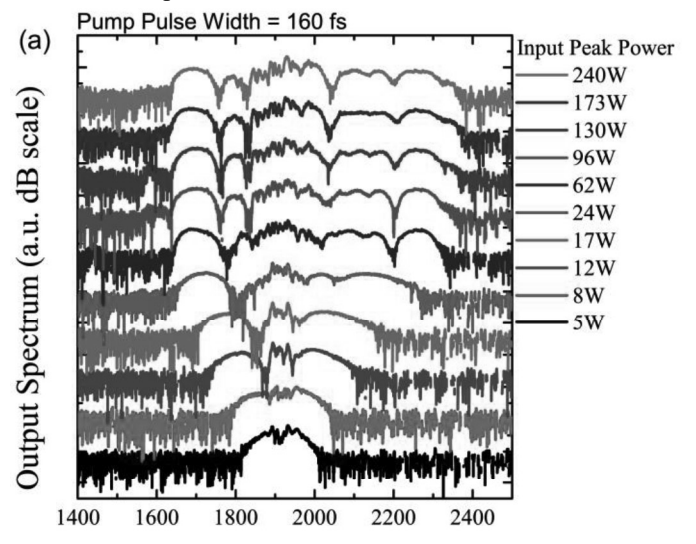


Fig. 2 Spectral broadening in a-Si:H waveguides at different coupled peak powers due to self-phase modulation. Figure reprinted with permission from [32], © 2010 OSA.

B. Supercontinuum Generation

Self-phase modulation, together with other Kerr effects such as modulation instability, soliton shift, and soliton fission, are employed to achieve wide spectral broadening and therefore generate a supercontinuum source. Reports on supercontinuum generation in a-Si:H waveguides have shown up to 790-nm wide coherent spectral broadening in the mid-IR regime [44] and 550-nm spectral broadening at telecommunication wavelengths [45], as shown in Fig. 3. Such broadband supercontinuum generation is critical to applications such as

optical frequency metrology, optical coherence tomography, and wavelength-division multiplexing. The large n_2 and resulting γ for a-Si:H can significantly reduce the power requirements for such demonstrations, thereby making chipbased SCG implementations more efficient.



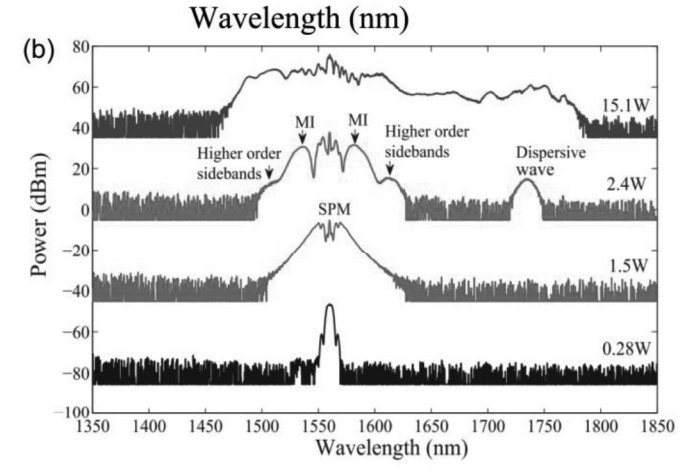


Fig. 3 a) Measured output spectrum in a 6-mm long a-Si:H waveguide for increasing peak powers with pulse duration of 160 fs, figure reproduced with permission from [44], © 2015 OSA; b) Measured output spectrum in a 1-cm long a-Si-H waveguide as function of on chip peak pump power with pulse duration of 1 ps, figure reproduced with permission from [45], © 2014 OSA.

C. All-Optical Wavelength Conversion

Optical wavelength conversion is a fundamental building block of many advanced optical processing systems. One implementation of wavelength conversion is an electro-optic converter, which consists of a detector followed by a laser that retransmits the incoming signal on the new wavelength. However, electro-optic converters are often undesirable as they are complex, bandwidth-limited, and lossy due to the optical-electrical-optical (OEO) conversion. Thus in many cases translating the information on the incoming wavelength to a new wavelength all-optically without entering the electrical domain is simpler and more efficient. All-optical wavelength converters are considered to be key processing components in the future high bandwidth networks, especially due to their potential use in wavelength division multiplexing (WDM) systems.

Four-wave mixing (FWM) is an important method to realize all-optical wavelength conversion, during which a new wave called the idler wave is generated with pump and signal waves input to the nonlinear medium. Much research has been focused on investigating FWM in a-Si:H waveguides[3][29][41][46]. Due to the high Kerr coefficient of a-Si:H, a maximum conversion efficiency of -13 dB at telecommunication data rates (10 GHz) using only 15 mW pump peak power and a conversion bandwidth as wide as 150 nm has been realized in an 8-mm long a-Si:H waveguide [3], as depicted in Fig. 4. Although the maximum FWM conversion efficiency in a-Si:H waveguides is comparable to similarly designed c-Si FWM demonstrations, the required pump power is 10 times less than c-Si [22] due to the large nonlinearity of a-Si:H, suggesting the capability of utilizing these devices for nonlinear optical applications with extremely low power requirements.

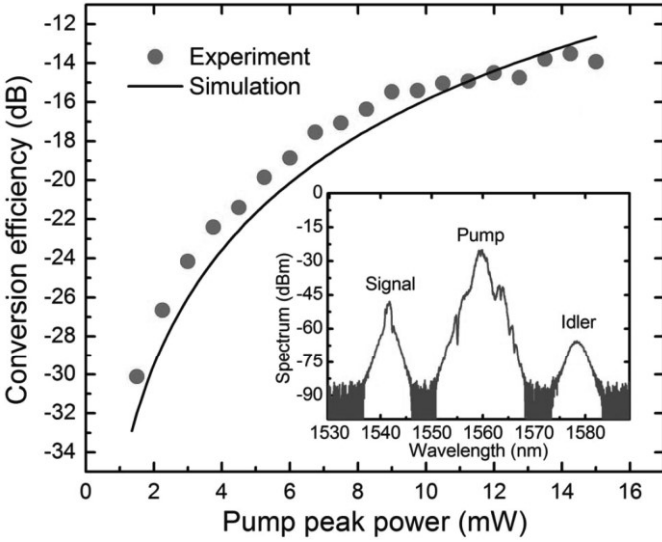


Fig. 4 Pulsed FWM experiment using a 10 GHz repetition-rate source; main: conversion efficiency as a function of pump peak power; inset: a sample FWM spectrum from a 8 mm a-Si:H waveguide when pump peak power is 8 mW. Figure reproduced with permission from [3], © 2012 OSA.

D. Optical Parametric Amplification and Oscillation

To compensate for the loss and restore the power of a signal in optical systems, optical amplification is critical. Ultrafast optical parametric processes, in which all energy is maintained in the form of photons (rather than lost through means such as electronic transitions, heat, or crystal vibrations), can provide an approach for signal amplification where amplification bandwidths can be very broad-band and defined through dispersion engineering. Additionally, the phase-dependent nature of the interaction can be exploited for phase-sensitive amplification with reduced noise figures over phase-insensitive approaches. The high FWM efficiency achieved in a-Si:H waveguides enables the possibility of using these devices for parametric amplification (OPA). Specifically, broadband on/off gain as high as 26.5 dB using 10 MHz laser source is reported in a 1.1 cm long a-Si:H waveguide [33] (Fig. 5a, 5b), and on-chip gain up to 10 dB at GHz-repetition rates is demonstrated in a 6 mm long a-Si:H waveguide as depicted in Fig. 5c [47]; in addition, the effect of source repetition rate is

studied in [8]. In comparison, the high TPA and FCA limit the parametric gain in a c-Si waveguide to 5.2 dB at a 75 MHz repetition rate [48].

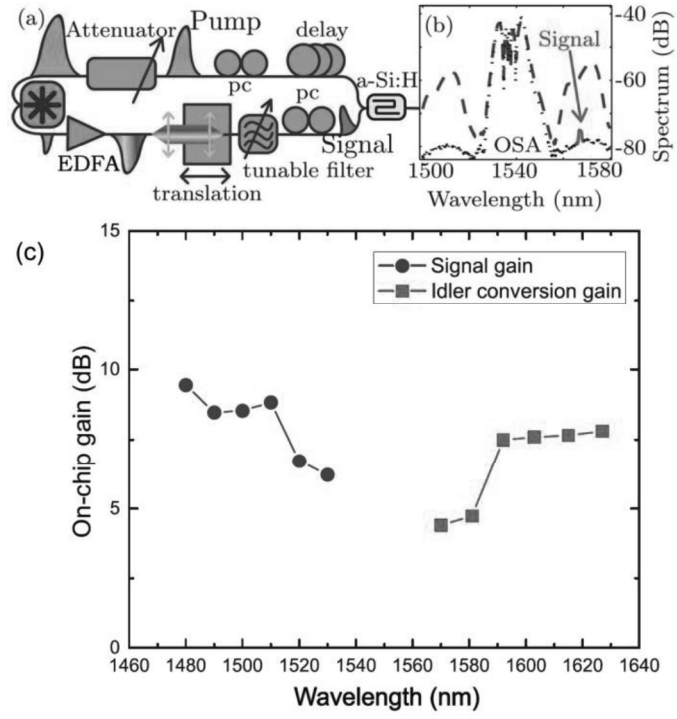


Fig. 5 a) and b) Experimental setup and output spectra for OPA test in an a-Si:H waveguide with 10 MHz pulses; black curve shows the case when pump and signal are not synchronized in time, blue curve is the case when pump and signal are synchronized, and a signal amplification of more than 20 dB is observed; figure reproduced with permission from [33], © 2011 OSA; c) Onchip gain / idler conversion at 1 GHz pump repetition rate as a function of signal wavelength in an a-Si:H waveguide, figure reproduced with permission from [47], © 2014 OSA.

Integrated tunable light sources are critical for on-chip optical systems; however, the indirect bandgap of silicon hampers the development of a light source in a conventional, electrically pumped manner. By placing the waveguide in a resonant-cavity, the broadband parametric gain described above can subsequently be employed to amplify vacuum fluctuations to achieve optical parametric oscillation (OPO), thereby providing a broadband tunable light source. The wavelength of the oscillating mode can be tuned by changing the cavity parameters (for example, by slightly changing the physical length of the dispersive cavity). As shown in Fig. 6, using a fixed 90 MHz pump wave, active wavelength tuning over 42 THz is achieved via optical parametric oscillation in a cavity with a 8 mm long a-Si:H waveguide as the nonlinear element [49]. The oscillation threshold of the pump energy is measured to be as low as 1.53 pJ. This represents the first silicon telecommunications-wavelength optical parametric oscillator.

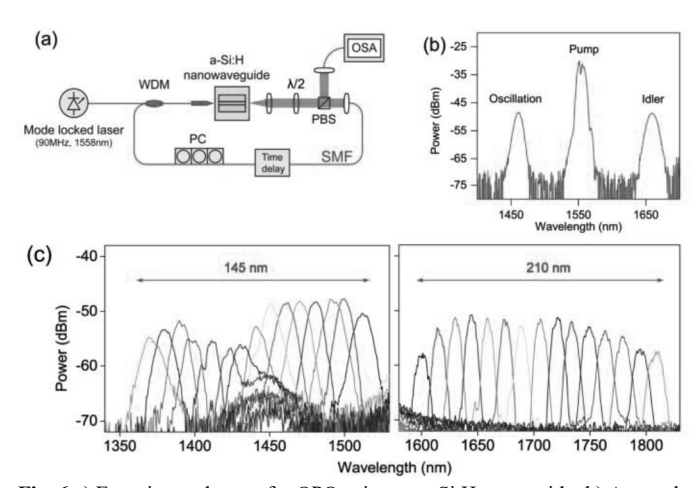


Fig. 6 a) Experimental setup for OPO using an a-Si:H waveguide; b) A sample optical spectrum of OPO; c) Tuning spectra of the oscillation mode at short wavelength side (1370 nm ∼1515 nm) and long wavelength side (1600 nm ~1810 nm) for a 1558-nm pump laser. Figure reproduced with permission from [49], © 2015 OSA.

E. Optical Time-Division Demultiplexing

Optical time division multiplexing (OTDM) is a technique that enables high transmission capacity of a fiber using a single optical carrier [50]. Much work in nonlinear integrated photonics has focused on demultiplexing high-speed OTDM signals [18][40][51][52]. To this end, the FWM process has the ability to efficiently transfer the information from a temporal section of the signal wave to the idler wave and thus inherently can be applied to realize OTDM demultiplexing. As depicted in Fig. 7, Ref. [40] reports error-free (BER < 10⁻⁹) 160-to-10 Gb/s OTDM demultiplexing in a 6-mm long a-Si:H waveguide using switching peak powers as low as 50 mW. Notably, this power requirement is one order of magnitude lower than demonstrations in other integrated photonic platforms such as chalcogenides [53][54] and c-Si [52][55].

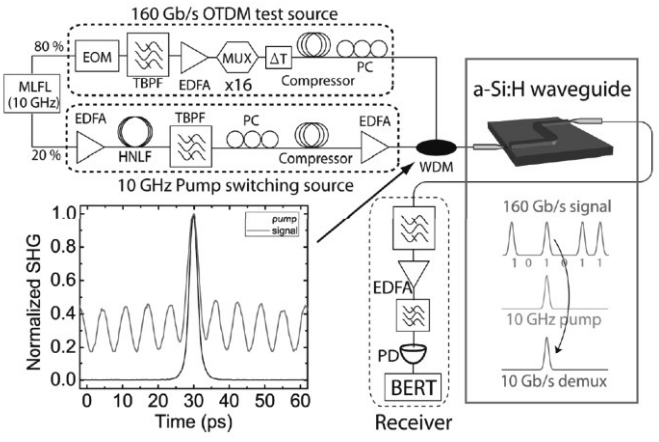


Fig. 7 Experimental setup for 160-to-10 Gb/s all-optical demutiplexing using an a-Si:H waveguide . Figure reprinted with permission from [40], © 2012 OSA.

F. All-Optical Switching

Another essential function required in future high bandwidth networks is all-optical switching. Although effects such as TPA and FCD can be employed to achieve all-optical switching, the required power is generally high and the operation speed is limited by the carrier lifetime [56]. The ultrafast response time of the Kerr effect makes it attractive for high data rate alloptical switching applications [14]. Cross-phase modulation (XPM) can be utilized to achieve high-speed all-optical switching in interferometric devices such as Mach-Zehnder interferometers [14] or optical resonators [57]. To this end, a-Si:H is a promising material to lower the power requirement for ultrafast all-optical switching. An initial demonstration was obtained in a-Si:H micro-cylindrical resonators [57], in which researchers realized all-optical switching with power thresholds as low as 5 µW (0.3 pJ of switching energy) and response time on the order of 10 ps. To further reduce the device size, a-Si:H integrated microring resonators have been utilized [15] to observe optical switching with response time of 14.8 ps and switching energy of only 720 fJ in an a-Si:H microring resonator with diameter of 10 µm. In comparison, the switching time of c-Si microring resonators is around 500 ps, as can be seen in Fig. 8. The speed of c-Si devices is restricted by the free carrier effect, while on the contrary, the free carrier effect can be negligible in a-Si:H microring resonators when operating with a high nonlinear FOM resulting in switching purely from XPM.

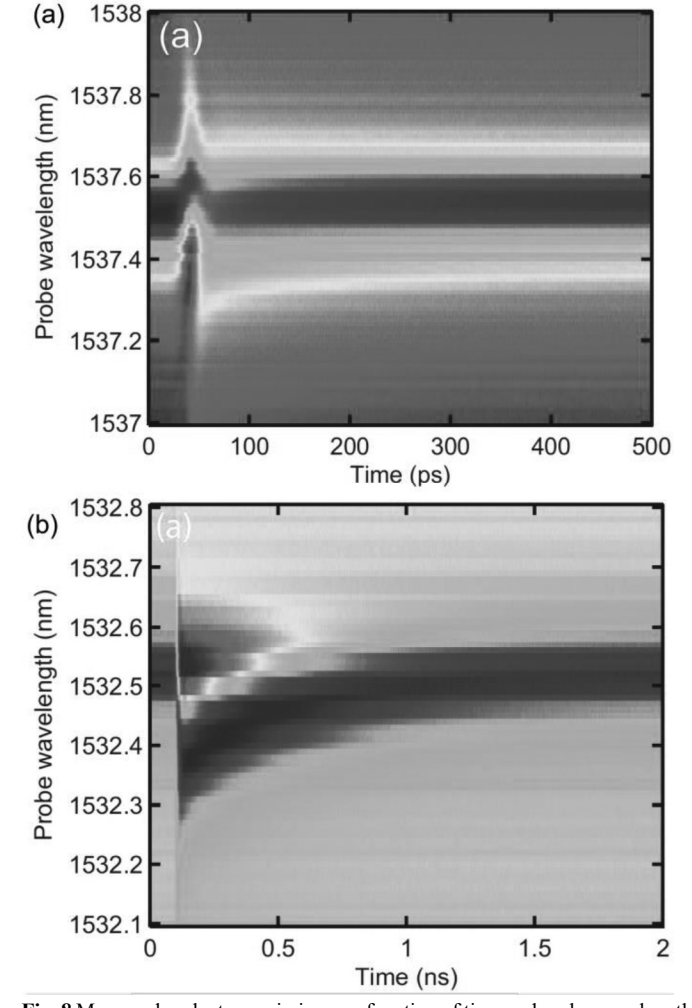


Fig. 8 Measured probe transmission as a function of time and probe wavelength in a) an a-Si:H microring resonator, b) a c-Si microring resonator. Red denotes high transmission and blue means low transmission. Figure reproduced with permission from [15], © 2014 OSA.

G. Photon Pair Generation

Quantum optics is a field studying how individual photons interact with atoms and molecules. Photons have been used to test many of the often counter-intuitive predictions of quantum mechanics, such as entanglement and teleportation, and are also an extremely useful resource for quantum information processing, especially for highly secure communications. Efficient photon pair generation is a critical building block for quantum optical systems, and researchers have made great efforts to achieve efficient photon pair generation in integrated quantum optical devices [58][59][60][61][62][63]. The large nonlinearity of a-Si:H makes it a promising material to realize high-quality photon pair generation via spontaneous four wave mixing (SFWM). The results in [64] show highly efficient photon-pair generation with a coincidence-to-accidental ratio (CAR) as high as 400 using an 8-mm long a-Si:H waveguide in far-detuned multiple wavelength channels, as depicted in Fig. 9. Notably, this CAR exceeds those achieved in both liquid nitrogen cooled dispersion shifted fiber (~30) [58] and c-Si (25-200) [59][60].

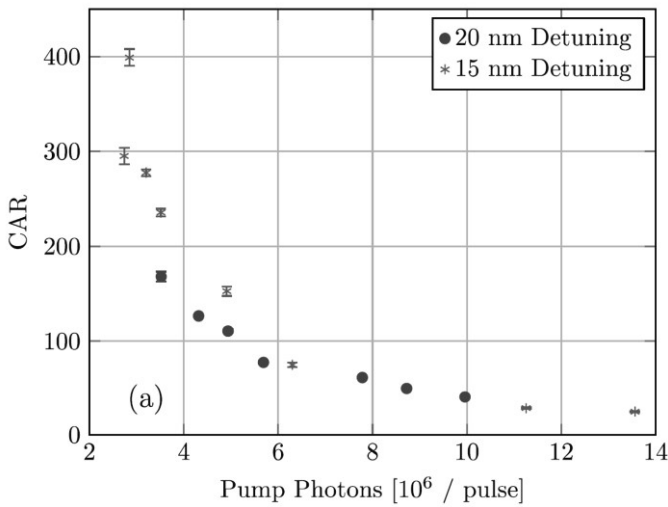


Fig. 9 Dark-count subtracted CAR versus the pump photon number per pulse. The highest CAR for the 15 nm (20 nm) detuning is 399 (168). Figure reproduced with permission from [64], © 2014 OSA.

H. Quantum Frequency Conversion

Another important building block in quantum optics is quantum frequency conversion, as in many optical systems the required photon frequencies differ from the frequencies at which the transmitters emit photons or the receivers detect them efficiently. Since the field of quantum optics studies the quantum states of photons, it is critical that the process utilized to realize frequency conversion is inherently noiseless; otherwise the excess noise can hinder the quantum process.

Two primary techniques are used to realize noiseless frequency conversion: one is frequency-down conversion via difference frequency generation (DFG) [65][66], and another is named four-wave mixing Bragg scattering (FWM-BS) [67][68][69][70]. DFG is a second-order nonlinear effect, in which a pump photon is down converted to a signal photon and an idler photon. In DFG, the energy of pump photon is nearly

twice that of signal photon and this means the pump and signal are far separated in wavelength. In contrast, FWM-BS is a thirdorder nonlinear effect and thus can be achieved in any material system and the wavelengths of the interacted waves can be closely spaced in wavelength. As depicted in Fig. 10, FWM-BS is a variant of the conventional FWM process. In conventional FWM, pump photons are annihilated in pairs and simultaneously sideband (signal and idler) photons are produced in pairs. However, the conventional process also enables the vacuum fluctuations associated with the signal and idler to be amplified so that excess noise is added to the signal and idler. In contrast, in FWM-BS, each generated idler photon results from an annihilated signal photon; thus, power is transferred directly from the signal to the idler, mirrored by the same power transfer between the two pumps. Because the total sideband power is constant, the vacuum fluctuations are not amplified, and hence no excess noise is produced. Notably, in FWM-BS the wavelengths of the generated idlers can be changed by tuning the wavelengths of the pumps and the signal without sacrificing the conversion efficiency, as long as the pumps and the signal are equally separated from the zero group velocity dispersion wavelength (phase matching condition, see Fig. 10b). This feature of FWM-BS allows flexible frequency conversion.

Low-noise frequency conversion via FWM-BS has been demonstrated in highly nonlinear fiber [67][68] and integrated platforms including c-Si waveguides [70] and silicon nitride waveguides [69]. However, the results are restricted in bandwidth (limited by fiber) or low internal conversion efficiency $(P_{b \ idler} + P_{r \ idler})/(P_{signal} + P_{b \ idler} + P_{r \ idler})$ (limited by the low Kerr coefficient and/or low nonlinear FOM). For example, a 5% internal conversion efficiency with 1 W and 55 mW pump peak powers was observed in a c-Si waveguide [70] and a 5% internal conversion efficiency with 6.8 W pump peak power was expected from simulation in a silicon nitride waveguide [69]. In contrast, a 67% internal conversion efficiency is achieved with only 81 mW (for pump1) and 285 mW (for pump2) peak powers in an a-Si:H waveguide [4]. Comparing these results, we can see that a-Si:H waveguides both require less pump power and yield higher efficiency than other silicon-based platforms, showing its great potential in quantum optical applications.

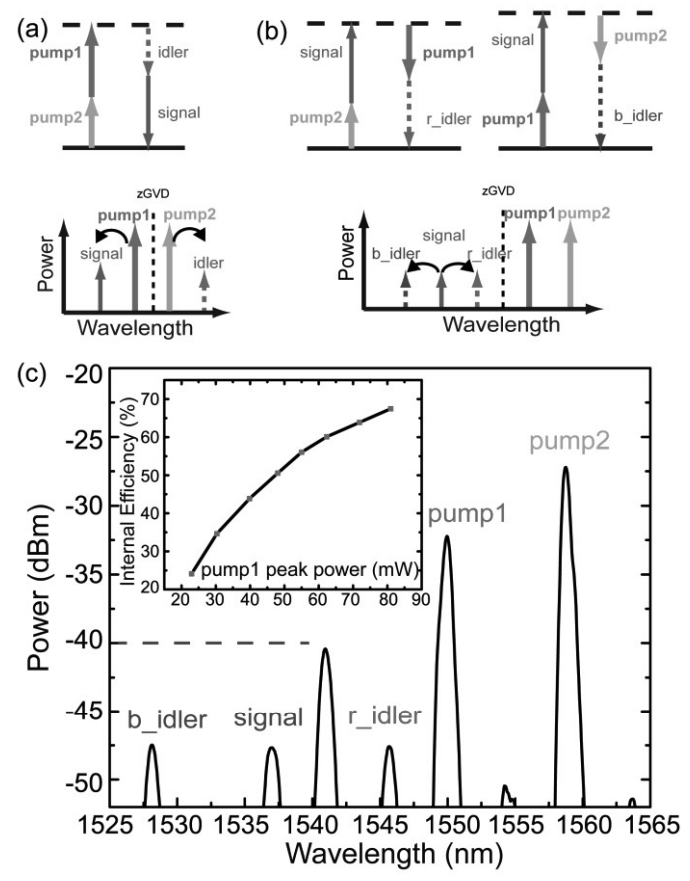


Fig. 10 a) In conventional non-degenerate FWM, a pump1 photon and a pump2 photon are annihilated, generating a signal photon and an idler photon; the zGVD wavelength is generally placed in the center of the four waves to achieve phase matching; b) In FWM-BS, a signal photon and a pump photon can be converted into another pump photon and an idler photon. Two idlers (b_idler and r_idler) are generated at different wavelengths; phase matching requires the zGVD wavelength to be in between the pumps and the signal; c) FWM-BS spectrum in a 8 mm a-Si:H waveguide with pump peak powers of 81 mW and 285 mW; inset: internal efficiency of FWM-BS as a function of pump1 peak power. Figure reproduced with permission from [4], © 2017 OSA.

IV. ALL-OPTICAL LOGIC GATES

All-optical logic functions are key elements to constructing efficient all-optical communication networks, since they serve as basic building blocks of optical devices for digital signal processing, storage, and encryption.

Integrated all-optical logic gates, including AND, NAND, XOR, and XNOR have been demonstrated using either thermopotic or carrier effects in microring resonators [24][71], and the Raman effect in waveguides [72], however, the operating speeds of these devices are restricted to less than 1 Gb/s due to the bandwidth of the resonators and response time of the nonlinear effects. To this end, parametric nonlinear processes such as FWM in integrated waveguide devices are especially promising to realize all-optical logic gates due to their ultrafast operation, low power requirement and potential for cascading to functional logic circuits. Specifically, up to 40-Gb/s all-optical XOR, XNOR, AND, and NOR gates utilizing FWM have been realized in c-Si waveguides [13][73].

The high nonlinearity and nonlinear FOM of a-Si:H allows for a highly efficient nonlinear interaction, and can be utilized to achieve more power-efficient high-speed all-optical logic gates. For example, based on the highly efficient FWM-BS process demonstrated in a-Si:H waveguides as described above, the energy of an input signal is transferred to idler waves with the help of the two incident pumps, leading to a depletion on the signal wave up to 7 dB [4][74]. This decrease of signal amplitude can be employed to yield a NAND logic operation, in which the logic inputs are encoded to the input pump waves via on-off keying (OOK), as depicted in Fig. 11a). Additionally, we can concurrently realize the AND logic functions through the generation of idlers in FWM-BS process, see Fig. 11a).

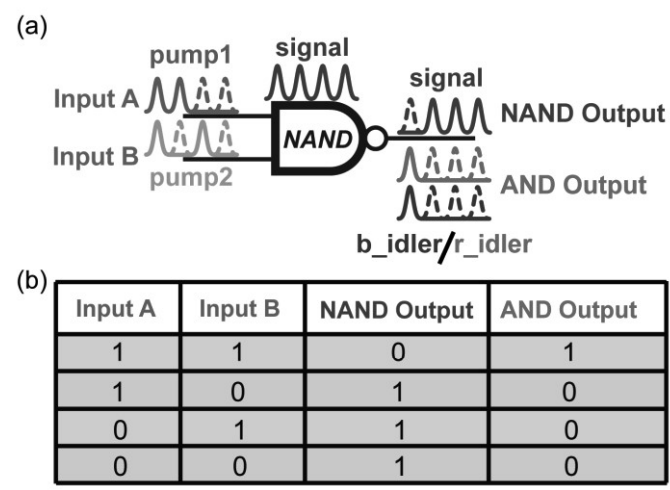


Fig. 11 a) NAND/AND logic gates design based on FWM-BS via OOK; b) the corresponding truth table.

The a-Si:H waveguide used in this logic gate experiment is 6-mm long with a cross-section of 420-nm (width) x 200-nm (height), and is designed to have a zero group velocity dispersion wavelength (zGVD) around 1550 nm for the transverse electric (TE)-like mode. The Kerr coefficient n_2 is determined to be around $5x10^{-17} m^2/W$ by FWM; the scanning electron microscope image of the waveguide is shown in Fig. 12b). We perform a preliminary FWM-BS test using a 90 MHz laser source, and the spectrum in Fig. 12 c) shows 7.4 dB amplitude depletion of the signal. Fig. 12 a) shows the experimental setup for time domain logic operation measurements. The source used in the experiment is a 5-GHz mode-locked laser followed by a pre-amplifier, and the spectrum is further broadened after propagating through the highly nonlinear fiber (HNLF); then a programmable optical filter (Finisar Waveshaper) is used to select the pumps (at 1550 nm and 1559 nm) and signal (at 1537 nm) waves each with a linewidth of 0.5 nm. An intensity modulator is used to reduce the rate of the pumps to 1.25 Gb/s, as well as to encode pseudo random binary sequences onto the pumps to serve as the logic inputs. After amplification, removing excess noise, and path matching, the three lightwaves are combined together and sent into the a-Si:H waveguide using a lensed fiber. Two lenses are then used to collect and couple the waveguide output into a single-mode fiber. Finally, a tunable filter is used to select each of the pumps, signal and idlers, and a photodiode followed by a sampling scope is used to obtain the time domain traces.

The experimental 1.25-Gb/s time domain logic results are shown in Fig. 12d). As can be seen, when both pumps are at

high levels (logic 1), the signal is depleted due to the FWM-BS process and hence exhibits a low level (logic 0); while with the absence of FWM-BS in all the other cases, the signal remains at high level (logic 1), thereby validating the all-optical NAND logic operation at the signal wavelength. The idlers behave in the inverse manner, and hence yield all-optical AND logic functions at the idler wavelengths (here we only show the red idler, as the blue idler behaves exactly the same as the red one). We can see from the time domain trace of the signal that the logic 0 level is more than 3 dB lower than logic 1 level for the NAND logic gate. Remarkably, the pump peak powers in the waveguide are around 85 mW, which is an order of magnitude less than our previous logic demonstration in HNLF [75]. In the a-Si:H waveguide, the extinction ratio of the signal (the difference between logic 1 and logic 0) and the operation speed are limited by the nonlinear loss due to TPA and carrier absorption, and we believe it can be increased by optimizing the a-Si:H deposition process.

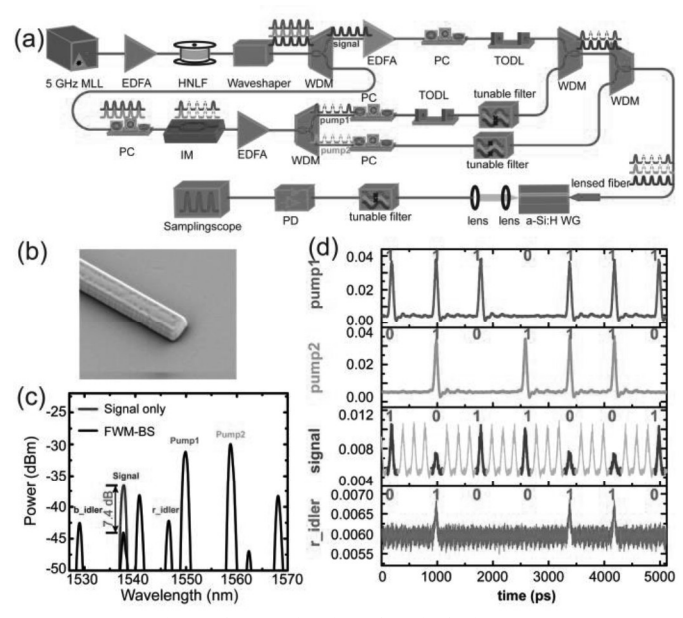


Fig. 12 a) Experimental setup for time domain logic measurements; MLL: mode-locked laser; EDFA: erbium doped fiber amplifier; WDM: wavelength division multiplexer; PC: polarization controller; TODL: tunable optical delay line; IM: intensity modulator; PD: photodiode; b) SEM image of the a-Si:H waveguide c) FWM-BS spectrum using a 90 MHz mode-locked laser as the source; d) Time domain logic operation measurement results.

Notably, the NAND gate is a universal logic gate and therefore can serve as a basic building block for all other logic gates. Despite the difference in the wavelengths of the logic output and input, cascaded logic operations can be easily achieved using our NAND gate design. Since the phase matching condition of the FWM-BS process allows the involved strong and weak waves to interchange between the pre-defined wavelengths without sacrificing the efficiency, simply filtering and amplifying the output waves will allow them to serve as inputs to subsequent gates. By design, each waveguide in a cascaded logic circuit can be identical, as the required phase matching condition is exactly the same in any configuration of the waves. As an example, Fig. 13 illustrates

an all-optical OR gate design using three NAND logic gates, for simplicity, only one idler is considered.

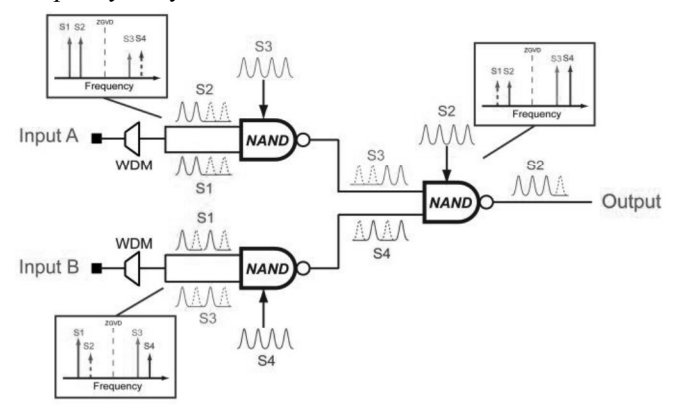


Fig. 13 Design of an all-optical OR gate using NAND logic gates based on FWM-BS. WDM: wavelength division multiplexer/demultiplexer. The top and bottom NAND gates have strong wave inputs conveying the same digital data patterns, respectively (S1-S2 for the top, S1-S3 for the bottom one).

V. A-SI:H MICRORING RESONATORS

As discussed above, FWM has been studied extensively for a wide range of applications. However, efficient FWM generally requires significant optical power and cm-long waveguide structures. To reduce power requirements and the device footprint, resonant enhancement in devices such as microring resonators can be employed. The resonant enhancement scales with the cavity finesse, which is inversely proportional to the linewidth of the employed resonance, resulting in a trade-off between the power requirement and the operational bandwidth (limited by the linewidth of the resonances). Therefore, a small cavity size is generally required to realize efficient high-speed operation. Additionally, a material with high nonlinearity is desired to reduce the required level of resonant enhancement and hence alleviate the trade-off between power and bandwidth. To this end, a-Si:H is a promising material to realize large bandwidth FWM in microring resonators due to its high refractive index and large nonlinearity.

The structure of our a-Si:H microring resonator device is illustrated in Fig. 14a). The 10-µm-radius ring is has a 200 nm gap from the bus waveguide, which has a total length of 3.8 mm; both the bus waveguide and the ring has a cross section of 250 nm (thickness) x 360 nm (width), which is designed to have a zGVD wavelength around 1550 nm for the TE-like mode [92].

The measured transmission spectrum of the a-Si:H microring is shown in the black line in Fig. 14b). Quasi-CW laser sources modulated at 10 GHz with a duty cycle of 1 to 6 are used in the FWM experiments. The pump is tuned into the resonance at 1548 nm, which has an extinction ratio of 11.3 dB and a 3-dB linewidth of 0.15 nm (18.7 GHz), corresponding to a Q factor of 10,300. The spectra at the bottom of Fig. 14b) show the FWM cases when both the pump and the signal are in the ring resonances (red curve) and when both are out of resonance (blue curve); in the out of resonance case, the FWM takes place in the 3.8-mm long bus waveguide. In this experiment, the input pump peak power in the waveguide is kept at 1.58 mW, and the input signal peak power is 37 μ W. The FWM conversion efficiency

in the ring is defined as the ratio of the output idler power $P_i^{(out)}$ to the input signal power $P_s^{(out)}$ (see Fig. 14a). According to the spectra, we obtain -34.6 dB FWM efficiency in the a-Si:H ring; compared to -57.4 dB in the bus waveguide, providing a 22.8 dB improvement in efficiency due to the ring resonant enhancement.

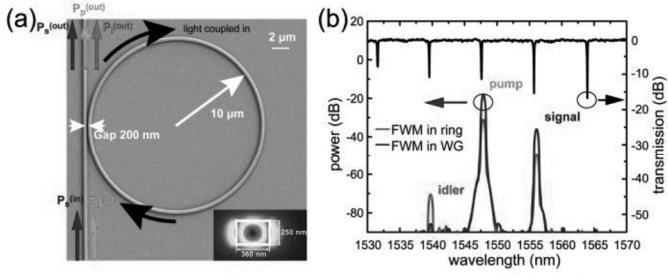


Fig. 14 a) SEM image of the microring resonator; inset: simulated electric field distribution of the waveguide TE-like mode; b) transmission spectrum and FWM spectra in the ring and waveguide; black line: normalized transmission spectrum of the microring; red line: spectrum of FWM in the ring resonator; blue line: spectrum of FWM in the waveguide.

The FWM conversion efficiency is measured with varying input pump peak powers while fixing the signal power at 37 μW, and the results are shown in Fig. 15a). As depicted with the red dots, at low pump powers, the FWM conversion efficiency can be improved by increasing the pump power, however, saturation begins at a pump power around 2 mW. An efficiency of -29.5 dB with only 4.3 mW pump power. We believe the conversion efficiency in the rings is limited mainly by the absorption of light due to the presence of carriers that are generated in the structures. However, this efficiency is higher than that achieved in c-Si microrings with similar size [76], suggesting that the nonlinear FOM of our a-Si:H film is higher than c-Si. Following the analysis described in [76], we simulate the FWM process in our a-Si:H microring resonator; as shown in Fig. 15a), the simulation is in good agreement with the experimental results, and we attribute the discrepancy at higher powers to the inaccurate estimation of the nonlinear loss. Finally, we compare the FWM efficiency when keep the pump in the same resonance and tune the signal to other resonant wavelengths, and the measured spectra are shown in Fig. 15b). As is shown, when the signal is in adjacent resonances at 1539 nm and 1564 nm, the efficiencies are comparable to the case in Fig. 14b), as expected from the low GVD design.

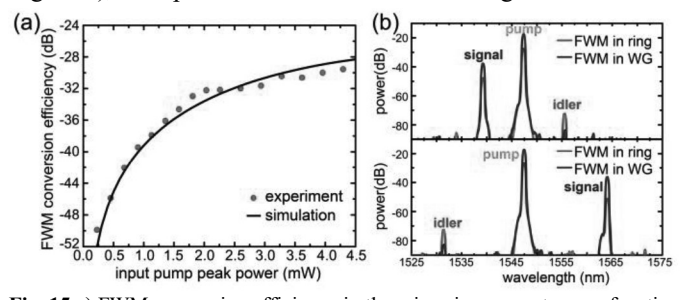


Fig. 15 a) FWM conversion efficiency in the microring resonator as a function of input pump power; red dots: experimental data; black line: simulation result; b) spectra of FWM with signal in different resonances; top: signal $\sim 1539~\rm nm;$ bottom: signal $\sim 1564~\rm nm.$

Compared to previous FWM demonstration in c-Si microrings with similar size [76], our device can achieve higher efficiency with lower Q factor and hence broader resonant linewidth, allowing for higher operational speed.

VI. CHALLENGES AND OPPORTUNITIES

It is logical to expect that TPA should vanish when the photon energy E_p is less than half the band gap energy $E_g/2$. As the band gap energy of a-Si:H can be tuned from 1.55 eV to 2.10 eV [39], it means that if the bandgap E_g of a-Si:H is higher than 1.6 eV, the photons at wavelength 1550 nm ($E_p \sim 0.8 \ eV$) should not be absorbed. However, due to the amorphous nature of the a-Si:H material, there are exponential band tails extending the absorption edge to photons with energy smaller than $E_g/2$ [77][78], resulting in TPA at a wavelength of 1550 nm even though the effective bandgap energy of a-Si:H is $\sim 1.7 \ eV$ [32].

Besides TPA, other non-instantaneous nonlinear absorption effects are found in some a-Si:H films. A popular mode used to explain the non-instantaneous absorption is the two-state absorption (TSA) model [79]. This model assumes that dangling bonds in a-Si:H induce mid-gap localized defect states, and sequential one-photon absorption events are facilitated by the existence of these mid-gap defect states. Although this model does provide a reasonable explanation, it is not commensurate with the experimental results reported in [42], and therefore some other phenomenological effects are likely in play. However, to the first order, the TSA model can help to approximate the interaction. Whatever the origin, the noninstantaneous nonlinear absorption can constrain the use of a-Si:H in nonlinear optical devices employing continuous wave light or long pulses with high repetition rates [79][80]. Fortunately, research has shown that lower deposition rates can help decrease the dangling bond defects and hence improve the material quality [15], likely as a result of the formation of Si-H bonds that a slower growth rate facilitates [36][77]. It is also found that the deposition temperature is a critical parameter in determining the film quality. As a consequence of the balance between the surface diffusion of the precursor SiH₄ and the desorption of hydrogen, the lowest defect density is usually achieved at a process temperature of around 250°C [81][82].

Another potential challenge of using a-Si:H for optical interconnects is light-induced degradation (often attributed to the Staebler-Wronski effect). In some a-Si:H devices, the waveguide properties and nonlinearity degrade over time at high optical intensities, likely due to the increase of defects in the material. The exact nature and cause of the Staebler-Wronski effect in a-Si:H is still not well understood, but the main material properties that could play a role in the effect are disorder in the Si network, hydrogen concentration and its complex bonding structure, as well as the concentration of impurities. A favorable mode to explain the effect is the hydrogen bond switching model. The mode proposes that the energy released by the recombination of photo-excited electrons and holes at weak Si-Si bond locations is sufficient to break the bond, and that a neighboring hydrogen atom then

forms a new bond with one of the Si atoms, preventing restoration of the broken bond and resulting in a dangling bond [83][84]. This effect is presumably associated with dangling bond defects. However, it has been shown that some types of degradation can be reversed through annealing [28].

Despite these challenges, a-Si:H creates great possibilities to realize low-power and large bandwidth CMOS-compatible alloptical signal processing devices as evidenced in the work highlighted in this manuscript. Due to the high Kerr coefficient and nonlinear FOM, a-Si:H devices can be utilized to achieve nonlinear interactions with power efficiencies and speeds that are impossible with other integrated platforms. For example, the parametric gain is limited to 5.2 dB at 75 MHz repetition rate in a c-Si waveguide due to the high TPA and FCA [48], while on-chip parametric gain as high as 17 dB has been demonstrated in an a-Si:H waveguide at a similar repetition rate of 90 MHz [49]. This superior performance enabled the only telecom-wavelength silicon optical parametric oscillator through the realization of net optical cavity gain [49]. The higher nonlinear FOM provided by a-Si:H also indicates that nonlinear phase shifts required for various parametric nonlinear optical processes can be achieved with lower input powers, resulting in more power-efficient processes. Additionally, due to the reduced impact of free carriers, a-Si:H microring resonators can enable ultrafast all-optical switching that is faster than c-Si resonators by more than an order of magnitude, as shown in Section III subsection F [15].

The beneficial nonlinear optical properties in a-Si:H also have significant implications in quantum information processing. The high FWM efficiency in an a-Si:H waveguide has enabled the generation of photon pairs with much higher CAR than other platforms, as discussed in Section III subsection G [64]. Additionally, as discussed in section III subsection H, the internal efficiency of FWM-BS in an a-Si:H waveguide can be as high as 67% at moderate power levels [4]; this high efficiency can be employed, for example, to demonstrate chip-based Hong-Ou-Mandel interference of two photons of different wavelengths (which requires at least 50% conversion efficiency) [85], which can be subsequently used to realize quantum copying without an ancilla [86].

Lastly, the simple growth process of a-Si:H film at low temperature allows for 3D integration, which can further reduce the size of integrated photonic devices and subsystems. Researchers have demonstrated direct fabrication of an a-Si:H photonic layer at the back-end of a CMOS wafer [87] and multiplane integration of a-Si:H photonic layers [88]. Furthermore, a-Si:H can facilitate heterogeneous integration with other material platforms [89][90]. For example, the material loss of silicon nitride photonic devices can be very low, which is preferable for signal transmission; however, the nonlinear coefficient is relatively low (one order smaller than c-Si). A device that combines the low loss property of silicon nitride and the relatively high nonlinearity of c-Si has been fabricated [90], with an interlayer coupling loss of only 0.02 dB at 1550. However, the fabrication process is very sophisticated, requiring wafer bonding, backside removal of the Si substrate and wet etching of the buried oxide layer. In contrast, replacing c-Si with a-Si:H helps to significantly simplify this heterogeneous fabrication process. The device can be built by first patterning the silicon nitride layer, followed by the deposition of silicon dioxide and chemical-mechanical polishing (CMP), producing a surface that is optimized for a-Si:H deposition and patterning of waveguides for nonlinear interactions [91].

VII. CONCLUSION

In conclusion, we have reviewed the recent progress in a-Si:H, a potential alternative to the c-Si film in an SOI stack, as an integrated optical platform for nonlinear optics. The beneficial nonlinear optical properties have enabled new functionalities in all-optical signal processing such as parametric gain in silicon at GHz data rates and ultrafast alloptical switching, that are critical in both emerging classical and quantum optical systems. Although there is greater variability in the material properties of a-Si:H due to its amorphous nature, understanding of the impact of growth conditions on these properties is emerging. The high nonlinear optical performance of a-Si:H devices combined with intrinsic compatibility with electronic-chip manufacturing (CMOS) and multilayer integration raises the prospect of practical platforms for future all-optical photonic integrated circuits requiring low cost, small footprint and low power consumption.

REFERENCES

- [1] H. Hu, E. Palushani, M. Galili, H. C. H. Mulvad, A. Clausen, L. K. Oxenlowe, and P. Jeppesen, "640 Gbit/s and 1.28 Tbit/s polarisation insensitive all optical wavelength conversion," *Opt. Express*, vol. 18, no. 10, pp. 9961–9966, 2010.
- [2] D. Hillerkuss, R. Schmogrow, T. Schellinger, M. Jordan, M. Winter, G. Huber, T. Vallaitis, R. Bonk, P. Kleinow, F. Frey, M. Roeger, S. Koenig, A. Ludwig, A. Marculescu, J. Li, M. Hoh, M. Dreschmann, J. Meyer, S. Ben Ezra, N. Narkiss, B. Nebendahl, F. Parmigiani, P. Petropoulos, B. Resan, A. Oehler, K. Weingarten, T. Ellermeyer, J. Lutz, M. Moeller, M. Huebner, J. Becker, C. Koos, W. Freude, and J. Leuthold, "26 Tbit/s line-rate super-channel transmission utilizing all-optical fast Fourier transform processing," Nat. Photonics, vol. 5, pp. 364–371, 2011.
- [3] K.-Y. Wang and A. C. Foster, "Ultralow power continuous-wave frequency conversion in hydrogenated amorphous silicon waveguides," *Opt. Lett.*, vol. 37, no. 8, pp. 1331–1333, 2012.
- [4] K. Li, H. Sun, and A. C. Foster, "Four-wave mixing Bragg scattering in hydrogenated amorphous silicon waveguides," *Opt. Lett.*, vol. 42, no. 8, pp. 1488–1491, 2017.
- [5] J. J. Wathen, P. Apiratikul, C. J. K. Richardson, G. A. Porkolab, G. M. Carter, and T. E. Murphy, "Efficient continuous-wave four-wave mixing in bandgap-engineered AlGaAs waveguides," *Opt. Lett.*, vol. 39, no. 11, pp. 3161–3164, 2014.
- [6] M. R. Dizaji, C. J. Krückel, A. Fülöp, P. A. Andrekson, V. Torres-Company, and L. R. Chen, "Silicon-rich nitride waveguides for ultrabroadband nonlinear signal processing," *Opt. Express*, vol. 25, no. 11, pp. 12100–12108, 2017.
- [7] X. Guan, H. Hu, L. K. Oxenløwe, and L. H. Frandsen, "Compact titanium dioxide waveguides with high nonlinearity at telecommunication wavelengths," *Opt. Express*, vol. 26, no. 2, pp. 1055–1063, 2018.
- [8] K.-Y. Wang and A. C. Foster, "GHz-rate optical parametric amplifier in hydrogenated amorphous silicon," J. Opt., vol. 17, p. 94012, 2015.
- [9] A. Bogoni, X. Wu, S. R. Nuccio, and A. E. Willner, "640 Gb/s all-optical regenerator based on a periodically poled lithium niobate waveguide," *J. Light. Technol.*, vol. 30, no. 12, pp. 1829–1834, 2012.
- [10] M. A. Ettabib, K. Bottrill, F. Parmigiani, A. Kapsalis, A. Bogris, M. Brun, P. Labeye, S. Nicoletti, K. Hammani, D. Syvridis, D. J.

- Richardson, and P. Petropoulos, "All-optical phase regeneration with record PSA extinction ratio in a low-birefringence silicon germanium waveguide," *J. Light. Technol.*, vol. 34, no. 17, pp. 3993–3998, 2016.
- [11] K. G. Petrillo, K.-Y. Wang, A. C. Foster, and M. a. Foster, "Highly sensitive ultrafast pulse characterization using hydrogenated amorphous silicon waveguides," *Opt. Express*, vol. 21, no. 25, p. 31229, 2013.
- [12] A. Bogoni, X. Wu, Z. Bakhtiari, S. Nuccio, and A. E. Willner, "640 Gbits/s photonic logic gates," *Opt. Lett.*, vol. 35, no. 23, pp. 3955–3957, 2010.
- [13] F. Li, T. D. Vo, C. Husko, M. Pelusi, D.-X. Xu, A. Densmore, R. Ma, S. Janz, B. J. Eggleton, and D. J. Moss, "All-optical XOR logic gate for 40Gb/s DPSK signals via FWM in a silicon nanowire," *Opt. Express*, vol. 19, no. 21, pp. 20364–20371, Oct. 2011.
- [14] C. Lacava, M. J. Strain, P. Minzioni, I. Cristiani, and M. Sorel, "Integrated nonlinear Mach Zehnder for 40 Gbit/s all-optical switching," Opt. Express, vol. 21, no. 18, pp. 21587–21595, 2013.
- [15] J. S. Pelc, K. Rivoire, S. Vo, C. Santori, D. A. Fattal, and R. G. Beausoleil, "Picosecond all-optical switching in hydrogenated amorphous silicon microring resonators," *Opt. Express*, vol. 22, no. 4, pp. 3797–3810, 2014.
- [16] V. Van, T. A. Ibrahim, K. Ritter, P. P. Absil, F. G. Johnson, R. Grover, J. Goldhar, and P.-T. Ho, "All-Optical Nonlinear Switching in GaAs AlGaAs Microring Resonators," *IEEE Photonics Technol. Lett.*, vol. 14, no. 1, pp. 74–76, 2002.
- [17] K.-Y. Wang, K. G. Petrillo, M. a. Foster, and A. C. Foster, "Ultralow-power all-optical processing of high-speed data signals in deposited silicon waveguides," *Opt. Express*, vol. 20, no. 22, p. 24600, 2012.
- [18] S. Suda, K. Tanizawa, T. Kurosu, T. Kamei, Y. Sakakibara, R. Takei, M. Mori, H. Kawashima, and S. Namiki, "Optical-time-division demultiplexing of 172 Gb/s to 43 Gb/s in a-Si:H waveguides," *IEEE Photonics Technol. Lett.*, vol. 26, no. 5, pp. 426–429, 2014.
- [19] Q. Lin, O. J. Painter, and G. P. Agrawal, "Nonlinear optical phenomena in silicon waveguides: modeling and applications," *Opt. Express*, vol. 15, no. 25, pp. 16604–16644, 2007.
- [20] M. A. Foster, A. C. Turner, M. Lipson, and A. L. Gaeta, "Nonlinear optics in photonic nanowires," *Opt. Express*, vol. 16, no. 2, pp. 1300– 1320, 2008.
- [21] D. J. Moss, R. Morandotti, A. L. Gaeta, and M. Lipson, "New CMOS-compatible platforms based on silicon nitride and Hydex for nonlinear optics," *Nat. Photonics*, vol. 7, pp. 597–607, Jul. 2013.
- [22] M. A. Foster, A. C. Turner, R. Salem, M. Lipson, and A. L. Gaeta, "Broad-band continuous-wave parametric wavelength conversion in silicon nanowaveguides," *Opt. Express*, vol. 15, no. 20, pp. 12949– 12958, 2007.
- [23] F. Da Ros, D. Vukovic, A. Gajda, K. Dalgaard, L. Zimmermann, B. Tillack, M. Galili, K. Petermann, and C. Peucheret, "Phase regeneration of DPSK signals in a silicon waveguide with reverse-biased p-i-n junction," *Opt. Express*, vol. 22, no. 5, pp. 5029–5036, Feb. 2014.
- [24] Q. Xu and M. Lipson, "All-optical logic based on silicon micro-ring resonators," Opt. Express, vol. 15, no. 3, pp. 924–929, 2007.
- [25] C. Doerr, L. Chen, D. Vermeulen, T. Nielsen, S. Azemati, S. Stulz, G. McBrien, X.-M. Xu, B. Mikkelsen, M. Givehchi, C. Rasmussen, and S.-Y. Park, "Single-chip silicon photonics 100-Gb/s coherent transceiver," Opt. Fiber Commun. Conf., vol. Th5C.1, 2014.
- [26] C. Zhang, S. Zhang, J. D. Peters, and J. E. Bowers, "8 × 8 × 40 Gbps fully integrated silicon photonic network on chip," *Optica*, vol. 3, no. 7, pp. 785–786, 2016.
- [27] S. Dutta, V. Agarwal, R. J. E. Hueting, J. Schmitz, and A. J. Annema, "Monolithic optical link in silicon-on-insulator CMOS technology," *Opt. Express*, vol. 25, no. 5, pp. 5440–5456, 2017.
- [28] B. Kuyken, H. Ji, S. Clemmen, S. K. Selvaraja, H. Hu, M. Pu, M. Galili, P. Jeppesen, G. Morthier, S. Massar, L. K. Oxenløwe, G. Roelkens, and R. Baets, "Nonlinear properties of and nonlinear processing in hydrogenated amorphous silicon waveguides," *Opt. Express*, vol. 19, no. 26, pp. B146–B153, Dec. 2011.
- [29] J. Matres, G. C. Ballesteros, P. Gautier, J.-M. Fédéli, J. Martí, and C. J. Oton, "High nonlinear figure-of-merit amorphous silicon waveguides," *Opt. Express*, vol. 21, no. 4, pp. 3932–3940, Feb. 2013.
- [30] Y. Shoji, T. Ogasawara, T. Kamei, Y. Sakakibara, S. Suda, K. Kintaka, H. Kawashima, M. Okano, T. Hasama, H. Ishikawa, and M. Mori, "Ultrafast nonlinear effects in hydrogenated amorphous silicon wire waveguide," *Opt. Express*, vol. 18, no. 6, pp. 5668–5673, 2010.
- [31] C. Grillet, L. Carletti, C. Monat, P. Grosse, B. Ben Bakir, S. Menezo,

- J. M. Fedeli, and D. J. Moss, "Amorphous silicon nanowires combining high nonlinearity, FOM and optical stability," *Opt. Express*, vol. 20, no. 20, pp. 22609–22615, 2012.
- [32] K. Narayanan and S. F. Preble, "Optical nonlinearities in hydrogenated-amorphous silicon waveguides," *Opt. Express*, vol. 18, no. 9, pp. 8998–9005, 2010.
- [33] B. Kuyken, S. Clemmen, S. K. Selvaraja, W. Bogaerts, D. Van Thourhout, P. Emplit, S. Massar, G. Roelkens, and R. Baets, "Onchip parametric amplification with 26.5 dB gain at telecommunication wavelengths using CMOS-compatible hydrogenated amorphous silicon waveguides," *Opt. Lett.*, vol. 36, no. 4, pp. 552–554, Feb. 2011.
- [34] C. Koos, L. Jacome, C. Poulton, J. Leuthold, and W. Freude, "Nonlinear silicon-on-insulator waveguides for all- optical signal processing," *Opt. Express*, vol. 15, no. 10, pp. 5976–5990, 2007.
- [35] H. K. Tsang and Y. Liu, "Nonlinear optical properties of silicon waveguides," Semicond. Sci. Technol., vol. 23, no. 64007, Jun. 2008.
- [36] X. Gai, D.-Y. Choi, and B. Luther-Davies, "Negligible nonlinear absorption in hydrogenated amorphous silicon at 1.55µm for ultrafast nonlinear signal processing," *Opt. Express*, vol. 22, no. 8, pp. 9948–9958, Apr. 2014.
- [37] C. Lacava, P. Minzioni, E. Baldini, L. Tartara, J. M. Fedeli, and I. Cristiani, "Nonlinear characterization of hydrogenated amorphous silicon waveguides and analysis of carrier dynamics," *Appl. Phys. Lett.*, vol. 103, p. 141103, 2013.
- [38] M. Dinu, "Dispersion of phonon-assisted nonresonant third-order nonlinearities," *IEEE J. Quantum Electron.*, vol. 39, no. 11, pp. 1498–1503, 2003.
- [39] K. Fukutani, M. Kanbe, W. Futako, B. Kaplan, T. Kamiya, C. M. Fortmann, and I. Shimizu, "Band gap tuning of a-Si:H from 1.55 eV to 2.10 eV by intentionally promoting structural relaxation," *J. Non. Cryst. Solids*, vol. 227–230, pp. 63–67, 1998.
- [40] K.-Y. Wang, K. G. Petrillo, M. A. Foster, and A. C. Foster, "Ultralow-power all-optical processing of high-speed data signals in deposited silicon waveguides," *Opt. Express*, vol. 20, no. 22, pp. 24600–24606, Oct. 2012.
- [41] S. Suda, K. Tanizawa, Y. Sakakibara, T. Kamei, K. Nakanishi, E. Itoga, T. Ogasawara, R. Takei, H. Kawashima, S. Namiki, M. Mori, T. Hasama, and H. Ishikawa, "Pattern-effect-free all-optical wavelength conversion using a hydrogenated amorphous silicon waveguide with ultra-fast carrier decay," *Opt. Lett.*, vol. 37, no. 8, pp. 1382–1384, 2012.
- [42] J. J. Wathen, V. R. Pagán, R. J. Suess, K.-Y. Wang, A. C. Foster, and T. E. Murphy, "Non-instantaneous optical nonlinearity of an a-Si:H nanowire waveguide.," *Opt. Express*, vol. 22, no. 19, pp. 22730– 22742, 2014.
- [43] O. Boyraz, T. Indukuri, and B. Jalali, "Self-phase-modulation induced spectral broadening in silicon waveguides," *Opt. Express*, vol. 12, no. 5, pp. 829–834, 2004.
- [44] H. Sun, K. Wang, R. Salem, P. Fendel, and A. C. Foster, "Coherent mid-IR supercontinuum generation in a hydrogenated amorphous silicon waveguide," *Conf. Laser Electr-optics*, vol. SM1P.6, 2015.
- [45] J. Safioui, F. Leo, B. Kuyken, S.-P. Gorza, S. K. Selvaraja, R. Baets, P. Emplit, G. Roelkens, and S. Massar, "Supercontinuum generation in hydrogenated amorphous silicon waveguides at telecommunication wavelengths," *Opt. Express*, vol. 22, no. 3, pp. 3089–3097, Feb. 2014.
- [46] C. Lacava, M. Ettabib, I. Cristiani, J. M. Fedeli, D. J. Richardson, and P. Petropoulos, "Ultra-Compact Amorphous Silicon Waveguide for Wavelength Conversion," *IEEE Photonics Technol. Lett.*, vol. 28, no. 4, pp. 410–413, 2016.
- [47] K.-Y. Wang and A. C. Foster, "GHz Near-IR Optical Parametric Amplifier using a Hydrogenated Amorphous Silicon Waveguide," Conf. Laser Electr-optics, vol. SW3I.7, 2014.
- [48] M. A. Foster, A. C. Turner, J. E. Sharping, B. S. Schmidt, M. Lipson, and A. L. Gaeta, "Broad-band optical parametric gain on a silicon photonic chip," *Nature*, vol. 441, pp. 960–963, Jun. 2006.
- [49] K.-Y. Wang, M. A. Foster, and A. C. Foster, "Wavelength-agile near-IR optical parametric oscillator using a deposited silicon waveguide," *Opt. Express*, vol. 23, no. 12, pp. 15431–15439, 2015.
- [50] H. Weber, R. Ludwig, S. Ferber, C. Schmidt-langhorst, M. Kroh, V. Marembert, C. Boerner, and C. Schubert, "Ultrahigh-Speed OTDM-Transmission Technology," J. Light. Technol., vol. 24, no. 12, pp. 4616–4627, 2006.
- [51] H. Ji, M. Pu, H. Hu, M. Galili, L. K. Oxenløwe, K. Yvind, J. M.

- Hvam, and P. Jeppesen, "Optical waveform sampling and error-free demultiplexing of 1.28 Tbit/s serial data in a nanoengineered silicon waveguide," *J. Light. Technol.*, vol. 29, no. 4, pp. 426–431, 2011.
- [52] F. Li, M. Pelusi, D.-X. Xu, a. Densmore, R. Ma, S. Janz, and D. J. Moss, "Error-free all-optical demultiplexing at 160Gb/s via FWM in a silicon nanowire," *Opt. Express*, vol. 18, no. 4, pp. 3905–3910, 2010.
- [53] L. P. Centre, "160 Gb/s optical time-division demultiplexing by four-wave mixing in a 5 cm length ultra-high nonlinear As2S3 waveguide," *Laser Phys.*, vol. 19, no. 1, pp. 2–3, 2006.
- [54] T. D. Vo, H. Hu, M. Galili, E. Palushani, J. Xu, L. K. Oxenløwe, S. J. Madden, D.-Y. Choi, D. a P. Bulla, M. D. Pelusi, J. Schröder, B. Luther-Davies, and B. J. Eggleton, "Photonic chip based transmitter optimization and receiver demultiplexing of a 1.28 Tbit/s OTDM signal.," Opt. Express, vol. 18, no. 16, p. Paper PDPC5, 2010.
- [55] H. Ji, H. Hu, M. Galili, L. K. Oxenløwe, M. Pu, K. Yvind, J. M. Hvam, and P. Jeppesen, "Optical Waveform Sampling and Error-free Demultiplexing of 1 . 28 Tbit / s Serial Data in a Silicon Nanowire," J. Light. Technol., vol. 29, no. 4, pp. 426–431, 2010.
- [56] V. R. Almeida, C. A. Barrios, R. R. Panepucci, M. Lipson, M. A. Foster, D. G. Ouzounov, and A. L. Gaeta, "All-optical switching on a silicon chip," Opt. Lett., vol. 29, no. 24, pp. 2867–2869, 2004.
- [57] N. Vukovic, N. Healy, F. H. Suhailin, P. Mehta, T. D. Day, J. V. Badding, and A. C. Peacock, "Ultrafast optical control using the Kerr nonlinearity in hydrogenated amorphous silicon microcylindrical resonators," Sci. Rep., vol. 3, no. 2885, pp. 1–5, 2013.
- [58] H. Takesue and K. Inoue, "1.5-µm band quantum-correlated photon pair generation in dispersion-shifted fiber: suppression of noise photons by cooling fiber," *Opt. Express*, vol. 13, no. 20, pp. 7832– 7839, 2005.
- [59] J. E. Sharping, K. F. Lee, M. A. Foster, A. C. Turner, B. S. Schmidt, M. Lipson, A. L. Gaeta, and P. Kumar, "Generation of correlated photons in nanoscale silicon waveguides," *Opt. Express*, vol. 14, no. 25, pp. 12388–12393, 2006.
- [60] K. Harada, H. Takesue, H. Fukuda, T. Tsuchizawa, T. Watanabe, K. Yamada, Y. Tokura, and S. Itabashi, "Generation of high-purity entangled photon pairs using silicon wire waveguide," *Opt. Express*, vol. 16, no. 25, pp. 20368–20373, 2008.
- [61] K. Harada, H. Takesue, H. Fukuda, T. Tsuchizawa, T. Watanabe, K. Yamada, Y. Tokura, and S. Itabashi, "Frequency and polarization characteristics of correlated photon-pair generation using a silicon wire waveguide," *IEEE J. Sel. Top. Quantum Electron.*, vol. 16, no. 1, pp. 325–331, 2010.
- [62] S. Clemmen, K. Phan Huy, W. Bogaerts, R. G. Baets, P. Emplit, and S. Massar, "Continuous wave photon pair generation in silicon-oninsulator waveguides and ring resonators," *Opt. Express*, vol. 17, no. 19, pp. 16558–16570, 2009.
- [63] M. Savanier, R. Kumar, and S. Mookherjea, "Photon pair generation from compact silicon microring resonators using microwatt-level pump powers," Opt. Express, vol. 24, no. 4, pp. 3313–3328, 2016.
- [64] K. Wang, V. G. Velev, K. F. Lee, A. S. Kowligy, P. Kumar, M. A. Foster, A. C. Foster, and Y. Huang, "Multichannel photon-pair generation using hydrogenated amorphous silicon waveguides," *Opt. Lett.*, vol. 39, no. 4, pp. 914–917, 2014.
- [65] K. De Greve, L. Yu, P. L. McMahon, J. S. Pelc, C. M. Natarajan, N. Y. Kim, E. Abe, S. Maier, C. Schneider, M. Kamp, S. Höfling, R. H. Hadfield, A. Forchel, M. M. Fejer, and Y. Yamamoto, "Quantum-dot spin-photon entanglement via frequency downconversion to telecom wavelength," *Nature*, vol. 491, pp. 421–425, 2012.
- [66] T. Kobayashi, R. Ikuta, S. Yasui, S. Miki, T. Yamashita, H. Terai, T. Yamamoto, M. Koashi, and N. Imoto, "Frequency-domain Hong—Ou–Mandel interference," *Nat. Photonics*, vol. 10, no. 7, pp. 441–444, 2016.
- [67] C. J. Mckinstrie, J. D. Harvey, S. Radic, and M. G. Raymer, "Translation of quantum states by four-wave mixing in fibers," *Opt. Express*, vol. 13, no. 22, pp. 9131–9142, 2005.
- [68] A. H. Gnauck, R. M. Jopson, C. J. McKinstrie, J. C. Centanni, and S. Radic, "Demonstration of low-noise frequency conversion by Bragg scattering in a fiber," *Opt. Express*, vol. 14, no. 20, pp. 8989–8994, 2006
- [69] I. Agha, S. Ates, M. Davanço, and K. Srinivasan, "A chip-scale, telecommunications-band frequency conversion interface for quantum emitters," *Opt. Express*, vol. 21, no. 18, pp. 21628–21638, 2013.
- [70] Y. Zhao, D. Lombardo, J. Mathews, and I. Agha, "Low control-power

- wavelength conversion on a silicon chip," *Opt. Lett.*, vol. 41, no. 15, pp. 3651–3654, 2016.
- [71] L. Zhang, R. Ji, L. Jia, L. Yang, P. Zhou, Y. Tian, P. Chen, Y. Lu, Z. Jiang, Y. Liu, Q. Fang, and M. Yu, "Demonstration of directed XOR/XNOR logic gates using two cascaded microring resonators," *Opt. Lett.*, vol. 35, no. 10, pp. 1620–1622, 2010.
- [72] M. N. V. Passaro and F. De Leonardis, "All-optical AND gate based on Raman effect in silicon-on-insulator waveguide," *Opt. Quantum Electron.*, vol. 38, pp. 877–888, 2006.
- [73] S. Gao, X. Wang, Y. Xie, P. Hu, and Q. Yan, "Reconfigurable dual-channel all-optical logic gate in a silicon waveguide using polarization encoding," *Opt. Lett.*, vol. 40, no. 7, pp. 1448–1451, 2015
- [74] K. Li, H. Sun, and A. C. Foster, "Ultra-low power signal depletion via four-wave mixing Bragg scattering in hydrogenated amorphous silicon waveguide," in *Conference on Laser and Electr-optics* (CLEO), 2016, p. FF2M.7.
- [75] K. Li, H.-F. Ting, M. A. Foster, and A. C. Foster, "High-speed all-optical NAND / AND logic gates using four-wave mixing Bragg scattering," Opt. Lett., vol. 41, no. 14, pp. 3320–3323, 2016.
- [76] A. C. Turner, M. A. Foster, A. L. Gaeta, and M. Lipson, "Ultra-low power parametric frequency conversion in a silicon microring resonator," *Opt. Express*, vol. 16, no. 7, pp. 4881–4887, 2008.
- [77] B. Tuttle and J. B. Adams, "Structure, dissociation, and the vibrational signatures of hydrogen clusters in amorphous silicon," *Phys. Rev. B*, vol. 56, no. 8, pp. 4565–4572, Aug. 1997.
- [78] L. Shen, N. Healy, P. Mehta, T. D. Day, J. R. Sparks, J. V. Badding, and A. C. Peacock, "Nonlinear transmission properties of hydrogenated amorphous silicon core fibers towards the mid-infrared regime," Opt. Express, vol. 21, no. 11, pp. 13075–13083, 2013.
- [79] K. Ikeda, Y. Shen, and Y. Fainman, "Enhanced optical nonlinearity in amorphous silicon and its application to waveguide devices," *Opt. Express*, vol. 15, no. 26, pp. 17761–17771, 2007.
- [80] X. Zeng, T. Tran, J. S. Pelc, D. Kielpinski, and R. G. Beausoleil, "Effects of non-instantaneous nonlinear absorption in hydrogenated amorphous silicon," *Conf. Laser Electr-optics*, vol. SM3R.6, 2016.
- [81] Z. E. Smith and S. Wagner, "Band tails, entropy, and equilibrium defects in hydrogenated amorphous silicon," *Phys. Rev. Lett.*, vol. 59, no. 6, pp. 688–691, 1987.
- [82] R. Takei, S. Manako, E. Omoda, Y. Sakakibara, M. Mori, and T. Kamei, "Sub-1 dB/cm submicrometer-scale amorphous silicon waveguide for backend on-chip optical interconnect," *Opt. Express*, vol. 22, no. 4, pp. 4779–4788, Feb. 2014.
- [83] M. Stutzmann, W. B. Jackson, and C. C. Tsai, "Light-induced metastable defects in hydrogenated amorphous silicon: a systematic study," *Phys. Rev. B*, vol. 32, no. 1, pp. 24–47, 1985.
- [84] A. . Kolodziej, "Staebler-Wronski effect in amorphous silicon and its alloys," *Opto-Electronics Rev.*, vol. 12, no. 1, pp. 21–32, 2004.
- [85] C. Joshi, A. Farsi, and A. Gaeta, "Hong-Ou-Mandel Interference in the Frequency Domain," Conf. Lasers Electro-Optics, p. FF2E.3, 2017
- [86] I. A. Khan and J. C. Howell, "Hong-Ou-Mandel cloning: Quantum copying without an ancilla," *Phys. Rev. A*, vol. 70, no. 10303, 2004.
- [87] J. M. Fedeli, L. Di Cioccio, D. Marris-Morini, L. Vivien, R. Orobtchouk, P. Rojo-Romeo, C. Seassal, and F. Mandorlo, "Development of silicon photonics devices using microelectronic tools for the integration on top of a CMOS wafer," Adv. Opt. Technol., vol. 2008, p. 412518, 2008.
- [88] J. Chiles, S. Buckley, N. Nader, S. W. Nam, R. P. Mirin, and J. M. Shainline, "Multi-planar amorphous silicon photonics with compact interplanar couplers, cross talk mitigation, and low crossing loss," APL Photonics, vol. 2, no. 11, p. 116101, 2017.
- [89] R. Takei, Y. Maegami, E. Omoda, Y. Sakakibara, M. Mori, and T. Kamei, "Low-loss and low wavelength-dependence vertical interlayer transition for 3D silicon photonics," *Opt. Express*, vol. 23, no. 14, pp. 18602–18610, 2015.
- [90] A. H. Hosseinnia, A. H. Atabaki, A. A. Eftekhar, and A. Adibi, "High-quality silicon on silicon nitride integrated optical platform with an octave-spanning adiabatic interlayer coupler," *Opt. Express*, vol. 23, no. 23, pp. 30297–30307, 2015.
- [91] M. Kossey, K. Li, H. Sun, and A. C. Foster, "Four-wave mixing in a multi-layer SiNx/a-Si:H photonic chip," *Conf. Laser Electr-optics*, p. STh31.5, 2018.
- [92] Simulations performed using OptiFDTD optiwave.com

13





Kangmei Li received the B.S. degree in physics in 2012 from Peking University, Beijing, China, and the M.S. degree in electrical and computer engineering in 2014 from Johns Hopkins University, Baltimore, Maryland, USA. She is currently working towards the Ph.D. degree in Integrated Photonics Laboratory at Johns Hopkins University. Her research interests include the development of ultra-wide bandwidth integrated photonic devices and high-speed optical communication systems.

Amy C. Foster was born in Rochester, New York and received her B.S. in electrical engineering from the University at Buffalo in Buffalo, New York in '03, and her M.S. and Ph.D. in electrical and computer engineering from Cornell University in Ithaca, New York in '07 and '09, respectively.

She is currently an Assistant Professor in the Electrical and Computer Engineering department at Johns Hopkins University in Baltimore, Maryland.

She has over 40 journal publications and over 70 conference proceedings in the area of silicon photonics. Her research has primarily focused on nanoscale-control of silicon-based integrated photonic waveguides for optimizing interactions such as nonlinear parametric processes. She is an Associate Editor of the OSA journal, *Optics Express*.

Prof. Foster has been a recipient of the DARPA Young Faculty Award, as well as the Johns Hopkins University Catalyst Award. She is a member of the Optical Society (OSA) and the American Physical Society (APS), and is serving on the IEEE Photonics Conference Optical Interconnects committee. She previously served as the Co-Director of the 49th Annual IEEE Conference on Information Sciences and Systems (2015).